Author/s:
Mohammadi, A;Manzie, C;Nesic, D

Title:
Online optimization of spark advance in alternative fueled engines using extremum seeking control

Date:
2014-08-01

Citation:
Mohammadi, A., Manzie, C. & Nesic, D. (2014). Online optimization of spark advance in alternative fueled engines using extremum seeking control. Control Engineering Practice, 29, pp.201-211. https://doi.org/10.1016/j.conengprac.2014.02.008.

Persistent Link:
https://hdl.handle.net/11343/299597

Online Optimization of Spark Advance in Alternative Fueled Engines Using Extremum Seeking Control ⋆

Alireza Mohammadi * **Chris Manzie** * **Dragan Nešić** **

* *Department of Mechanical Engineering*
(e-mail: a.mohammadi@pgrad.unimelb.edu.au and manziec@unimelb.edu.au),
** *Department of Electrical and Electronic Engineering*
(e-mail: dnesic@unimelb.edu.au),
University of Melbourne, Parkville, 3010, Victoria, Australia.

Abstract: Alternative fueled engines offer greater challenges for engine control courtesy of uncertain fuel composition. This makes optimal tuning of input parameters like spark advance extremely difficult in most existing ECU architectures. This paper proposes the use of grey-box extremum seeking techniques to provide real-time optimization of the spark advance in alternative fueled engines. Since practical implementation of grey-box extremum seeking methods are typically done using digital technology, this paper takes advantage of emulation design methods to port the existing continuous-time grey-box extremum seeking methods to discrete-time frameworks. The ability and flexibility of the proposed discrete-time framework is demonstrated through simulations and in practical situation using a natural gas fueled engine.

Keywords: Engine control, Extremum seeking, Optimization, Parameter estimation, Alternative fuels.

1. INTRODUCTION

Nowadays, due to the increasingly demanding emissions legislation and growing concerns about the shortage of petroleum resources, the research and development into alternative fuels for automotive application has become an important subject. Alternative fuels such as ethanol and methanol mixtures, LPG (Liquified Petroleum Gas), and CNG (Compressed Natural Gas) have lower fuel costs and cleaner exhaust gas emissions as compared with gasoline and diesel, see Kim et al. (2009). These fuels may also enhance energy security through increasing sources of reliable energy.

However, despite all of these advantages, the main drawback of these fuels is that their composition can vary depending on origin, season, and relative cost. The results of a study by Ly (2002) established significant variations between supply sources within large geographic areas such as Europe and Australia.

The change in composition of these fuels was found to affect the performance and emissions of alternative fueled engines, see Min et al. (1998). The main reason is that current approaches to control of engines rely on static maps for steady-state operating points. In these methods, the optimum values of variables, such as spark timing and air/fuel ratio, are stored in a memory in engine control unit (ECU) for a finite number of engine operating set-points. Since the values of optimal control variables in the static maps are obtained for a specific fuel composition, if the fuel composition changes then the values are no longer optimal. Alternatively, the fuel composition must be sensed using fuel sensors and calibration of the maps undertaken for all possible compositions. Consequently, the former approach results in suboptimal engine performance at any operating point, while latter involves more cost and calibration effort. Both are undesirable.

This points to the need for online adaptation in order to optimize the engine performance after refueling if fuel composition is changed. Extremum seeking (ES) controllers typically provide online optimization in the presence of plant dynamics and slowly time-varying uncertainties. Moreover, they are computationally very simple which is beneficial for online implementation and also have the advantage of rigorous theoretical guarantees. As a result, they warrant investigation as a potential solution to the fuel composition problem described above.

Extremum seeking (ES) is an adaptive control approach for real-time optimization of the steady-state operating condition in cases when the plant model or performance function is not fully known but instead the value of performance function can be measured by probing the system (Krstić et al. (2003)). Therefore, the goal of extremum seeking control is to tune the system inputs online so that it operates in the vicinity of this extremum in steady-state. Due to the advantage of rigorous theoretical guarantees of

⋆ This work was supported by Australia Research Council Discovery Grant, DP0985388. A shorter version of this paper appeared in the Proceedings of the *IFAC Workshop on Engine and Powertrain Control, Simulation and Modeling*, Rueil-Malmaison, France, 2012, Mohammadi et al. (2012).

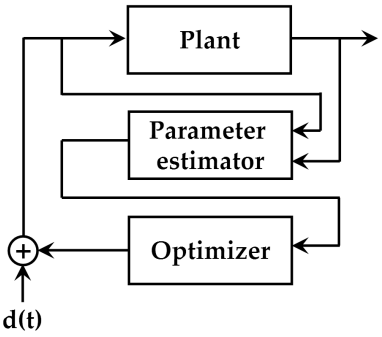

Fig. 1. General structure of a grey-box extremum seeking controller

ES controllers and their simple computational implementation, they have many applications (Tan et al. (2010)).

There are two main approaches for design of ES controllers. First there are methods which treat the system as a black-box, which for many applications means potentially disregarding known information about the model structure (Popovic et al. (2006), Killingsworth et al. (2009), Hellström et al. (2013)). The second approach, which is used in this paper, incorporates a known plant structure with uncertain parameters in the online optimization of plant operation, referred to as a grey-box ES controller. In this latter approach, as shown in Fig. 1, the input of the plant is subjected to a perturbation and the resulting output perturbations are used to update estimates of the plant parameters. The updated parameter estimates are then used in an optimization scheme to update the input to the plant.

One of the early research works on grey-box ES in engine control has been used by Scotson and Wellstead (1990) to optimize the brake torque of a spark ignition engine as a function of the spark advance. Zarrop and Romments (1993) extended the results derived by Wellstead and Scotson to the multi-input case. The lack of a rigorous convergence analysis in all of these attempts has limited the ability to guarantee much about the system performance. Egardt and Larsson (2005) used the same approach of Wellstead and Scotson for exactly the same application but they analyzed the role of probing in the control law and asymptotic properties of the grey-box ES controller. Nevertheless, their results are presented for particular classes of plants and particular optimization and estimation algorithms are used to achieve extremum seeking.

Nešić et al. (2013) proposed a general framework for design of grey-box ES controllers. This framework provides precise conditions under which a large class of continuous optimization algorithms can be combined with a large class of parameter estimators to achieve convergence of the closed loop trajectories to the desired extremum. This enables different combinations of parameter estimators and optimization algorithms without sacrificing the robustness of the closed-loop system. This framework also allows us through simulations to select algorithms that are better suited for an application at hand. However, the results of Nešić et al. (2013) are presented in continuous-time while practical implementations of engine controllers are in discrete-time.

This paper takes advantage of emulation design methods to introduce a discrete-time analog of the continuous-time ES framework proposed in Nešić et al. (2013). Emulation of a system consists of two steps: (1) the design of a continuous-time controller for a continuous-time plant using known continuous-time design methods to satisfy closed-loop control performance objectives, and (2) the discretization and implementation of the continuous-time controller using sample and hold devices with the objective of obtaining comparable closed-loop system properties Pierre et al. (1995). Emulation control of nonlinear systems has been widely investigated in the literature Qu (1998), Teel et al. (1998), Owens et al. (1990). However, due to the singularly perturbed structure of the ES schemes, the existing results cannot be used directly. Due to the time scale separation required for averaging and singular perturbation in stability analysis of continuous-time ES controllers, some parameters should be tuned appropriately in the closed-loop system. The emulation design method also introduces sample period as additional tuning parameter.

The first objective of this paper is to develop a tuning procedure for grey-box ES controller parameters including sample period to ensure that the discretized controller preserves the closed-loop performance of the continuous-time controller under sampling. To this end, first the continuous-time closed-loop controller is stabilized with tuning parameters in the estimation and optimization algorithms and also choosing an appropriate dither signal. The amplitude and frequency of the dither signal play an important role in the controller performance regarding convergence speed and accuracy as illustrated in detail by Tan et al. (2008). Then, sample time is adjusted such that certain conditions are satisfied that guarantee stability of the discrete-time ES controller.

The second objective of this study is to maximize the brake torque of a natural gas fueled engine by finding the best spark advance using the proposed discrete-time grey-box ES controller in the presence of varying fuel composition. For this purpose, first some simulations have been performed based on the data collected from open-loop tests on the engine to test combinations of estimation and optimization algorithms, satisfying the required conditions of the framework. A subset of the promising combinations are then validated on a real engine running at fixed speed and torque in a dynamometer test cell for natural gas switched between two possible blends.

In the next section, some background information on the grey-box ES control is provided. The proposed emulation design method is detailed in Section 3 . Section 4 describes the experimental setup. The procedure of using discrete-time grey-box ES controller for spark advance optimization is outlined in Section 5 . Simulation and experimental results are illustrated in Section 6 and 7, respectively. Conclusions are presented in Section 8, followed by a proof of the main result in the Appendix.

2. THE FRAMEWORK FOR CONTINUOUS-TIME GREY-BOX ES CONTROLLER

In this section, first the grey-box ES framework for dynamic plants is summarized from Nešić et al. (2013).

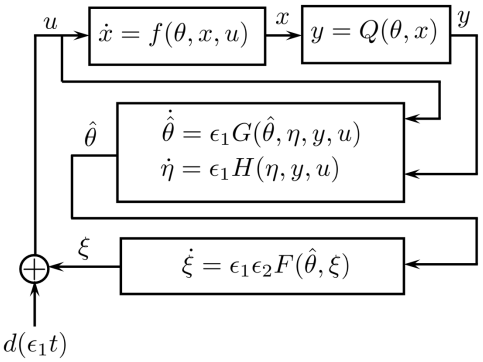

Fig. 2. The framework for grey-box ES schemes Nešić et al. (2013)

Then, different estimation and optimization algorithms that satisfy conditions of the framework are provided and a particular combination of these algorithms is used to illustrate the verification of conditions of the framework.

Notation: The set of real numbers is denoted by $\mathbb{R}$. The continuous function $\alpha : [0, a) \to \mathbb{R}_{\geq 0}$ is said to belong to class $\mathcal{K}$ if it is nondecreasing and zero at zero. The continuous function $\alpha : \mathbb{R}_{\geq 0} \to \mathbb{R}_{\geq 0}$ is said to be of class $\mathcal{K}_\infty$ if it is strictly increasing, unbounded and zero at zero.

2.1 Grey-box ES Controller for Dynamic Plants

Consider the continuous-time closed-loop system with a nonlinear dynamic plant Nešić et al. (2013):

$$\begin{aligned}
\dot{x} &= f(\theta, x, u) \ , && (1)\\
y &= Q(\theta, x) \ , && (2)\\
u &= \xi + d(\epsilon_1 t) \ , && (3)\\
\dot{\hat{\theta}} &= \epsilon_1 \ G(\hat{\theta}, \eta, y, u) \ , && (4a)\\
\dot{\eta} &= \epsilon_1 \ H(\eta, y, u) \ , && (4b)\\
\dot{\xi} &= \epsilon_1 \ \epsilon_2 \ F(\hat{\theta}, \xi), \qquad \epsilon_1, \ \epsilon_2 > 0, && (5)
\end{aligned}$$

where $x \in \mathbb{R}^n$ is the plant state, $\theta \in \mathbb{R}^p$ is a fixed unknown parameter vector, $u \in \mathbb{R}^m$ is the input, $y \in \mathbb{R}$ is the output, $d(\epsilon_1 t)$ is a dither signal that is typically chosen so that appropriate parameter convergence can be achieved and ξ comes from the optimization algorithm (5). The optimization algorithm uses the estimated parameter $\hat{\theta}$ that is obtained from the estimator (4a), (4b). The parameter estimation algorithm (4a) may contain extra states $\eta \in \mathbb{R}^q \times \mathbb{R}^s$ to widen the class of estimators considered, and ϵ_1 and ϵ_2 are tuning parameters of the estimator and optimization scheme, respectively. Note that the stability analysis of this system requires time scale separation between plant, estimator and optimizer. As a result, by fine tuning ϵ_1 and ϵ_2, there are three time scales, where the plant is the fastest subsystem, $\hat{\theta}$ is the medium system and ξ is the slow system. Fig. 2 shows the relations between different parts of the closed-loop system (1)-(5).

Consider $x = \ell(\theta, u)$ as a unique solution of $0 = f(\theta, x, u)$ and assume that the map

$$h(\theta, u) := -Q(\theta, \ell(\theta, u))$$

has an extremum at $u = \xi^*$.

Writing the closed loop system in coordinates $\tilde{x} := x - \ell(\theta, u), \tilde{\theta} := \hat{\theta} - \theta, \tilde{\eta} := \eta - \eta^*, \tilde{\xi} := \xi - \xi^*$ gives

$$\begin{aligned}
\dot{\tilde{x}} &= f(\theta, \tilde{x} + \ell(\theta, \tilde{\xi} + \xi^* + d(\epsilon_1 t)), \tilde{\xi} + \xi^* + d(\epsilon_1 t)) \\
&\quad -\epsilon_1 \epsilon_2 \frac{\partial \ell}{\partial u} F(\tilde{\theta} + \theta, \tilde{\xi} + \xi^*) \\
&=: \widetilde{f}(\epsilon_1 t, \tilde{x}, \tilde{\theta}, \tilde{\xi}, \epsilon_1 \epsilon_2) && (6)\\
\dot{\tilde{\theta}} &= \epsilon_1 \ G(\tilde{\theta} + \theta, \tilde{\eta} + \eta^*, Q(\theta, \tilde{x} + \ell(\theta, \tilde{\xi} + \xi^* + d(\epsilon_1 t))), \\
&\quad \tilde{\xi} + \xi^* + d\,(\epsilon_1 t)) \\
&=: \epsilon_1 \ \widetilde{G}(\epsilon_1 t, \tilde{\eta}, \tilde{x}, \tilde{\theta}, \tilde{\xi}) && (7a)\\
\dot{\tilde{\eta}} &= \epsilon_1 \ H(\tilde{\eta} + \eta^*, Q(\theta, \tilde{x} + \ell(\theta, \tilde{\xi} + \xi^* + d(\epsilon_1 t))), \\
&\quad \tilde{\xi} + \xi^* + d\,(\epsilon_1 t)) \\
&=: \epsilon_1 \ \widetilde{H}(\epsilon_1 t, \tilde{\eta}, \tilde{x}, \tilde{\xi}) && (7b)\\
\dot{\tilde{\xi}} &= \epsilon_1 \ \epsilon_2 \ F(\tilde{\theta} + \theta, \tilde{\xi} + \xi^*) \\
&=: \epsilon_1 \ \epsilon_2 \ \widetilde{F}(\tilde{\theta}, \tilde{\xi}) \ . && (8)
\end{aligned}$$

Then, the following assumption guarantees that the continuous-time grey-box ES scheme (1)-(5) is stable and converges to optimum value of the performance function (2).

Assumption 1. The continuous-time closed-loop system (1)-(5) is practically asymptotically stable uniformly in ϵ_1 and ϵ_2, i.e., there exist $\Delta > 0$ and a Lyapunov candidate $V(\tilde{x}, \tilde{\theta}, \tilde{\eta}, \tilde{\xi})$ such that for any strictly positive real number $\nu > 0$ there exist $\omega \in \mathcal{K}_\infty$ and $\epsilon_1^*, \epsilon_2^* > 0$ such that for all $\epsilon_1 \in (0, \epsilon_1^*)$ and $\epsilon_2 \in (0, \epsilon_2^*)$ the following holds:

$$\begin{aligned}
\frac{\partial V}{\partial \tilde{x}} \widetilde{f} + \frac{\partial V}{\partial \tilde{\theta}} (\epsilon_1 \widetilde{G}) + \frac{\partial V}{\partial \tilde{\eta}} (\epsilon_1 \widetilde{H}) + \frac{\partial V}{\partial \tilde{\xi}} (\epsilon_1 \epsilon_2 \widetilde{F}) \\
\leq -\omega(\tilde{x}, \tilde{\theta}, \tilde{\eta}, \tilde{\xi}) + \nu, \qquad (9)
\end{aligned}$$

for all $|\tilde{x}(t_0), \tilde{\theta}(t_0), \tilde{\eta}(t_0), \tilde{\xi}(t_0)| \leq \Delta$ and for all $t \geq t_0 \geq 0$.

Sufficient conditions under which Assumption 1 holds are presented in Nešić et al. (2013). The results of Nešić et al. (2013) also provide a prescriptive framework for extremum seeking controller design that combines a large class of optimization methods with a large class of parameter estimation schemes that satisfy Assumption 1. The following subsections provide a range of algorithms for parameter estimator and optimizer and conditions for a particular estimator and optimizer that guarantee satisfaction of Assumption 1.

2.2 Estimation Algorithms (EA)

In order to estimate the unknown parameters in (1), (2) different type of parameter estimators in form of (4a), (4b) can be employed which satisfy required conditions of Assumption 1. Some examples from Nešić et al. (2013) are:

- EA1. Gradient algorithm,
- EA2. Gradient algorithm with integral cost function,
- EA3. Pure least-squares algorithm,
- EA4. Recursive least-squares algorithm.

While all of these algorithms can be shown to satisfy Assumption 1, this is only demonstrated explicitly here for the recursive least-squares algorithm (EA4). Note that

for cases when it is known that different parameters are likely to change with different rates, a Kalman filter may be more suitable choice than the RLS Soderstrom et al. (1997).

For this purpose, a specific type of plant is required. So consider the following class of steady-state maps that are linearly parameterized with θ as

$$y = \phi^T(u)\theta := h(\theta, u). \tag{10}$$

For this plant, the parameter update using EA4 is given by

$$\dot{\hat{\theta}} = -P\phi(u)(y - \phi(u)^T\hat{\theta}) := G(\hat{\theta}, y, u) \tag{11a}$$
$$\dot{P} = \gamma P - P\phi(u)\phi(u)^T P := H(P, u) \tag{11b}$$

where $\gamma \geq 0$ and P is the error covariance matrix. Using $u = \xi + d(t)$ and writing (11a) and (11b) in coordinates $\tilde{\theta} = \hat{\theta} - \theta$, $\tilde{P} = \hat{P} - P^*$ and $\tilde{\xi} = \xi - \xi^*$ gives:

$$\begin{aligned}\dot{\tilde{\theta}} &= -(\widetilde{P} + P^*)\phi\tilde{\theta} \\ &:= \widetilde{G}(\tilde{\theta}, \widetilde{P}, \tilde{\xi}) \end{aligned} \tag{12a}$$
$$\begin{aligned}\dot{\widetilde{P}} &= \gamma(\widetilde{P} + P^*) - (\widetilde{P} + P^*)\phi\phi^T(\widetilde{P} + P^*) \\ &:= \widetilde{H}(t, \widetilde{P}, \tilde{\xi}) \end{aligned} \tag{12b}$$

According to (Nešić et al., 2013, Proposition 10), Assumption 1 holds for the estimator (12a), (12b) if $\phi(t)$ is persistently exciting, i.e., for all $t_0 \geq 0$ there exists $\mu, \sigma > 0$ such that

$$\int_{t_0}^{t_0+\sigma} \phi(\tau)\phi^T(\tau)d\tau \geq \mu I. \tag{13}$$

By using an appropriate dither signal $d(t)$, $\phi(t)$ can be made persistently exciting.

In the next subsection optimization algorithms that can be combined with estimation algorithms in this subsection to satisfy Assumption 1 are provided.

2.3 Optimization Algorithms (OA)

Similar to the previous subsection, there exists a large class of optimization algorithms which satisfy the conditions of Assumption 1; some examples from Nešić et al. (2013) are:

- OA1. Gradient descent algorithm,
- OA2. Continuous Newton method,
- OA3. Continuous Jacobian matrix transpose,
- OA4. Combination of Newton and gradient methods,
- OA5. Levenberg-Marquardt method,
- OA6. Newton-Raphson-Ben-Israel.

In order to demonstrate the verification of Assumption 1, the continuous Jacobian matrix transpose method (OA3) is chosen as the optimization algorithm:

$$\dot{\xi} = -\Gamma J_r^T(\hat{\theta}, \xi)\nabla h(\hat{\theta}, \xi) \tag{14}$$
$$:= F(\hat{\theta}, \xi)\ , \tag{15}$$

where $\nabla h(\xi)$ denotes the gradient of h at ξ, J_r represents the Jacobian of $r(\xi) = \nabla h(\xi)$ and Γ is an arbitrary positive definite matrix. Then, writing (15) in coordinates $\tilde{\theta} = \hat{\theta} - \theta$ and $\tilde{\xi} = \xi - \xi^*$ gives:

$$\begin{aligned}\dot{\tilde{\xi}} &= -F(\tilde{\theta} + \theta, \tilde{\xi} + \xi) \\ &:= \widetilde{F}(\tilde{\theta}, \tilde{\xi}) \end{aligned} \tag{16}$$

The above optimization algorithm, according to (Nešić et al., 2013, Proposition 3), satisfies Assumption 1 if the Jacobian matrix $J_r(\xi)$ is invertible in some neighborhood of ξ^*.

Up to this point, the existing continuous-time grey-box ES framework and algorithms fitted to this framework are explained. In the next section, the discrete-time analog of this framework is investigated.

3. DISCRETE-TIME GREY-BOX ES FRAMEWORK

In this section, first emulation design methods are explained for the general form of the plant, parameter estimator and optimization algorithm and the main result is stated. Then, the main result is applied to the particular estimator and optimizer explained in the previous section.

3.1 Emulation Design of the Grey-box ES Framework

Emulation of a controller involves discretizing a continuous-time controller design using sample and hold devices. Fig. 3 shows the zero-order hold equivalent of the continuous time controller. Therefore, the exact discretization of the parameter estimator (7a), (7b) and optimization algorithm (8) are obtained as:

$$\begin{aligned}\tilde{\theta}^e(k+1) &= \tilde{\theta}^e(k) \\ &\quad + \int_{kT}^{(k+1)T} \epsilon_1 \widetilde{G}(\epsilon_1\tau, x(k), \tilde{\theta}(\tau), \tilde{\eta}(\tau), \tilde{\xi}(k))d\tau \\ &=: \widetilde{G}_T^e(k, x(k), \tilde{\theta}(k), \tilde{\eta}(k), \tilde{\xi}(k), \epsilon_1) \end{aligned} \tag{17a}$$
$$\begin{aligned}\tilde{\eta}^e(k+1) &= \tilde{\eta}^e(k) \\ &\quad + \int_{kT}^{(k+1)T} \epsilon_1 \widetilde{H}(\epsilon_1\tau, x(k), \tilde{\eta}(\tau), \tilde{\xi}(k))d\tau \\ &=: \widetilde{H}_T^e(k, x(k), \tilde{\eta}(k), \tilde{\xi}(k), \epsilon_1) \end{aligned} \tag{17b}$$
$$\begin{aligned}\tilde{\xi}^e(k+1) &= \tilde{\xi}^e(k) + \int_{kT}^{(k+1)T} \epsilon_1\epsilon_2 \widetilde{F}(\tilde{\theta}(k), \tilde{\xi}(\tau))d\tau \\ &=: \widetilde{F}_T^e(\tilde{\theta}(k), \tilde{\xi}(k), \epsilon_1\epsilon_2) \end{aligned} \tag{18}$$

where T denotes the sampling period, $\tilde{\theta}^e$, $\tilde{\eta}^e$ and $\tilde{\xi}^e$ are exact discrete values of the continuous-time states $\tilde{\theta}$, $\tilde{\eta}$ and $\tilde{\xi}$.

Due to the introduction of the new tuning parameter T and also due to the fact that, in general, it is impossible to compute $\widetilde{G}_T^e$, $\widetilde{H}_T^e$ and $\widetilde{F}_T^e$ exactly, an approximate discrete-time model of the controller should be used:

$$\tilde{\theta}^a(k+1) = \widetilde{G}_T^a(k, \tilde{x}(k), \tilde{\theta}(k), \tilde{\eta}(k), \tilde{\xi}(k), \epsilon_1) \tag{19a}$$
$$\tilde{\eta}^a(k+1) = \widetilde{H}_T^a(k, \tilde{x}(k), \tilde{\eta}(k), \tilde{\xi}(k), \epsilon_1) \tag{19b}$$
$$\tilde{\xi}^a(k+1) = \widetilde{F}_T^a(\tilde{\theta}(k), \tilde{\xi}(k), \epsilon_1\epsilon_2) \tag{20}$$

which are obtained from (6), (7a), (7b) and (8) using one of many possible numerical integration methods (e.g. Runge-Kutta) and $\tilde{\theta}^a$, $\tilde{\eta}^a$ and $\tilde{\xi}^a$ are approximate discrete-time values of the continuous-time states $\tilde{\theta}$, $\tilde{\eta}$ and $\tilde{\xi}$.

In the ensuing sections, the following discrete-time model of the plant is used:

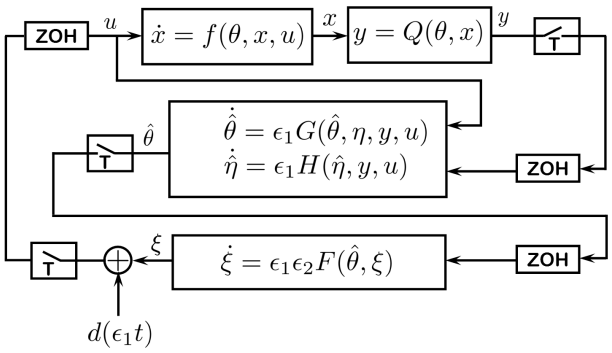

Fig. 3. Sample and zero order hold devices in the grey-box ES framework

$$\tilde{x}(k+1) = \int_{kT}^{(k+1)T} \widetilde{f}(\epsilon_1\tau, \tilde{x}(\tau), \tilde{\theta}(k), \tilde{\xi}(k), \epsilon_1\epsilon_2)d\tau$$
$$=: \widetilde{f}_T(k, \tilde{x}(k), \tilde{\theta}(k), \tilde{\xi}(k), \epsilon_1\epsilon_2). \quad (21)$$

Before stating the main result, some conditions are presented that guarantee the mismatch between the exact discrete-time model of the controller and its approximation is small.

3.2 Consistency Conditions

In order to guarantee that the mismatch between the exact discrete-time model of the grey-box ES controller (17a), (17b) and (18) and its approximation (19a), (19b) and (20) is small, the conditions of Assumption 1 are not enough and some form of consistency should be considered (Laila et al. (2002)). To this end, first one-step consistency is defined for a general nonlinear continuous-time system $\dot{\psi}(t) = \Psi(\psi(t))$ and its exact and approximate discretization as $\psi^e(k+1) = \Psi^e_T(\psi^e(k))$ and $\psi^a(k+1) = \Psi^a_T(\psi^a(k))$, respectively. Then, the required condition is stated based on the consistency definition.

Definition 1. $\Psi^a(\psi^a(k))$ is one-step consistent with $\Psi^e(\psi^e(k))$ if there exist Δ such that for any $|\psi| < \Delta$, there exists T^* such that for all $T \in (0, T^*)$ the following holds:

(1) Ψ^a_T is one-step consistent with $\Psi^{Euler}_T := \psi + T\Psi$, i.e., there exists a function $\rho \in \mathcal{K}_\infty$ such that:
$$|\Psi^a_T - \Psi^{Euler}_T| \leq T\rho(T)$$
(2) there exist $M > 0$ and $\gamma \in \mathcal{K}_\infty$ such that for all $|\psi| < \Delta$ and $|\zeta| < \Delta$:
- $|\Psi(\zeta)| \leq M$
- $|\Psi(\zeta) - \Psi(\psi)| \leq \gamma(|\zeta - \psi|)$. □

Now the following assumption is considered for the exact and approximate discretization of the estimation and optimization algorithms.

Assumption 2. For any given $\epsilon_1 \in (0, \epsilon_1^*)$, $\epsilon_2 \in (0, \epsilon_2^*)$, the approximate discrete-time controller $\widetilde{G}^a_T(k, \tilde{x}, \tilde{\theta}, \tilde{\eta}, \tilde{\xi}, \epsilon_1)$, $\widetilde{H}^a_T(k, \tilde{x}, \tilde{\eta}, \tilde{\xi}, \epsilon_1)$ and $\widetilde{F}^a_T(\tilde{\theta}, \tilde{\xi}, \epsilon_1\epsilon_2)$ are one-step consistent with the exact discrete-time controller $\widetilde{G}^e_T(k, \tilde{x}, \tilde{\theta}, \tilde{\eta}, \tilde{\xi}, \epsilon_1)$, $\widetilde{H}^e_T(k, \tilde{x}, \tilde{\eta}, \tilde{\xi}, \epsilon_1)$ and $\widetilde{F}^e_T(\tilde{\theta}, \tilde{\xi}, \epsilon_1\epsilon_2)$. □

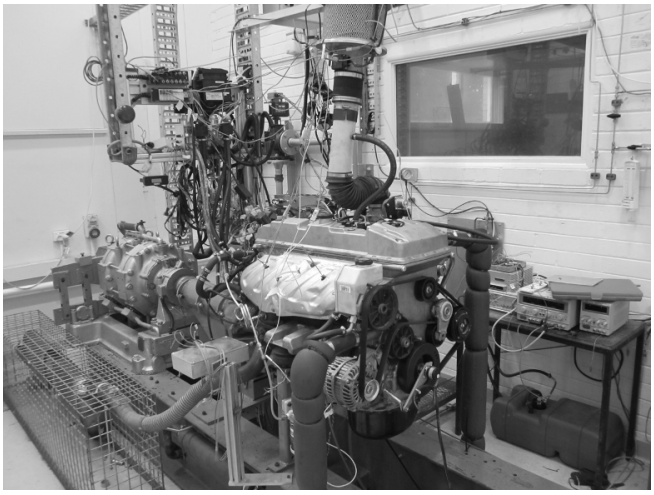

Fig. 4. Natural gas fueled engine used in the experiments

3.3 Main Result

Here the main result states the conditions under which the approximate discrete-time model (19a), (19b) and (20) of the continuous-time ES controller (7a), (7b) and (8) is a valid discrete-time controller for the continuous-time plant (6) and preserves stability property of the continuous-time controller under sampling.

Theorem 1. Suppose that Assumptions 1 and 2 hold. Let Δ and ω come from Assumption 1 and arbitrary $\widehat{\nu}$ is given. Then, there exist $\epsilon_1^*, \epsilon_2^*$ such that for any fixed $\epsilon_1 \in (0, \epsilon_1^*)$, $\epsilon_2 \in (0, \epsilon_2^*)$ there exists T^* such that for all $T \in (0, T^*)$, the following holds for the approximate discrete-time closed-loop system (19a)-(21):

$$\frac{\Delta V}{T} = \frac{V(\tilde{x}(k+1), \tilde{\theta}(k+1), \tilde{\eta}(k+1), \tilde{\xi}(k+1))}{T}$$
$$- \frac{V(\tilde{x}(k), \tilde{\theta}(k), \tilde{\eta}(k), \tilde{\xi}(k))}{T} \leq -\omega(\tilde{x}, \tilde{\theta}, \tilde{\eta}, \tilde{\xi}) + \widehat{\nu} \quad (22)$$

for all $|(\tilde{x}_0, \tilde{\theta}_0, \tilde{\eta}_0, \tilde{\xi}_0)| \leq \Delta$ and all $k \geq 0$.

Proof: See Appendix.

Remark 2. The property (22) guarantees practical asymptotic stability of the closed-loop system (19a)-(21).

Remark 3. The tuning procedure according to Theorem 1 is as follows. For any desired accuracy of the approximate discrete-time closed-loop system (19a)-(21) characterized by $\widehat{\nu}$, first the parameters ϵ_1 and ϵ_2 are adjusted to deliver appropriate convergence of the continuous-time scheme. Then, the sample period T should be tuned so that for all initial conditions in the ball $\mathcal{B}_\Delta$:

- The system state x converges to the $\mathcal{B}_{\hat{\nu}}$ ball centered at the equilibrium point of the plant in time scale kT;
- The parameter estimate $\hat{\theta}$ converges to the $\mathcal{B}_{\hat{\nu}}$ ball centered at the true value of the parameter θ in the slower time scale $\epsilon_1 kT$;
- The optimizer state ξ converges in the slowest time scale $\epsilon_1\epsilon_2 kT$ to the $\mathcal{B}_{\hat{\nu}}$ ball centered at the optimal value ξ^*.

4. EXPERIMENTAL FACILITIES

All experiments were conducted in the test cell of the ACART Laboratory at the University of Melbourne. The engine used for the experiments was a six cylinder 4L Ford Falcon BF MY2006 gasoline engine which is shown in Fig. 4 with specifications in Table 1. This engine is modified using a Prins Compressed Natural Gas Vapor Sequential Injection kit (VSI-CNG) to operate with natural gas for the controller implementation. While the fuel used in these experiments is CNG, this information is not used by the controller and so the methodologies presented here are equally applicable to other fuels with variable composition such as LPG and ethanol-gasoline blends. The optimization algorithm is performed based on the feedback signal (e.g. brake torque in this study) to find the optimum engine control variable.

Table 1. Engine specifications

Manufacture	Ford of Australia
Type	6 cylinder/water cooled
Firing order	1-5-3-6-2-4
Valve train	Dual Independent VCT
Max brake torque	393 Nm at 2500 RPM
Max power	190 kW at 5200 RPM

In order to keep the speed and load of the engine constant, an eddy current dynamometer is used which can only work as a brake and is not capable of motoring the engine. The air-fuel ratio was maintained at an approximately stoichiometric condition by adjusting the injection duration with feedback from a wide-band exhaust oxygen gas sensor. The response time of this sensor is 5ms which can be considered negligible in comparison to sample time of 5sec in the ES controller. The proposed ES algorithms were implemented in MATLAB. The output of the MATLAB program were sent in real-time directly to the engine control unit (ECU) via ATI Vision software, thereby adapting the stored calibration. The maximum delays in communication between MATLAB and ATI and ECU and ATI were measured at approximately 6ms, which was considered negligible in the context of this application.

Feedback torque was obtained through measurements from a load cell on the dynamometer, which is clearly not practical for real world driving. This approach enables the ES methodology to be demonstrated without additional complications introduced by online torque estimation. Methods utilizing in-cylinder pressure measurements have been proposed for providing torque feedback in practice (e.g Park and Sunwoo (2003) and Leonhardt et al. (1999)), however at this point in time are not typically developed in engines, and therefore, online torque estimation is recognized as a future area of interest. Furthermore, with the additional scope provided by in-cylinder measurement, there are opportunities to use other estimates such as CA50 for feedback (Glaser and Powell (1981)) to improve the ES convergence and overall engine performance.

The torque measurement was averaged over a period of three seconds to minimize the effects of combustion variability and measurement noise. The sample rate of the load cell is 0.1sec. The sample rate used by the controller

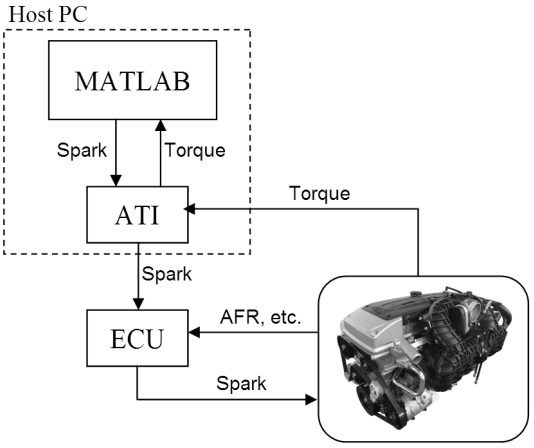

Fig. 5. Configuration of the experimental setup

was set nominally to five seconds so as to be longer than the torque measurement time. Fig. 5 depicts the configuration of the experimental setup.

5. ES CONTROLLER DESIGN FOR THE SPARK ADVANCE OPTIMIZATION

Spark timing is an important parameter in engine performance and emissions. The objective of spark timing (spark advance) control is to find the crank angle position where the mixture of air and fuel in compression stroke should be ignited to produce the maximum brake torque (MBT), called MBT spark timing. In this section, using some experimental tests, it is shown that the composition of natural gas effects the MBT spark advance. Then, based on the obtained data a parameterized model of the plant is presented. Having the structure of the plant, the discrete-time grey-box ES controller is designed for online optimization of the spark advance as fuel composition is varying.

5.1 The effect of fuel composition variation on the MBT spark advance

The experiments are carried out for two different test gases of compositions presented in Table 2. The test gases used were selected to reflect the extreme variation in composition of natural gases distributed in large geographic areas like Europe and Australia (Ly (2002)). In addition, these compositions represent two extreme laminar flame speeds for natural gas and consequently extreme variation in the MBT spark advance is expected, see Oostendorp and Levinsky (1990) for more details.

Table 2. Composition of test gas fuels

	Gas A	Gas B
Methane	100	80
Ethane	0	2
Propane	0	0.5
Carbon Dioxide	0	9
Nitrogen	0	8.5

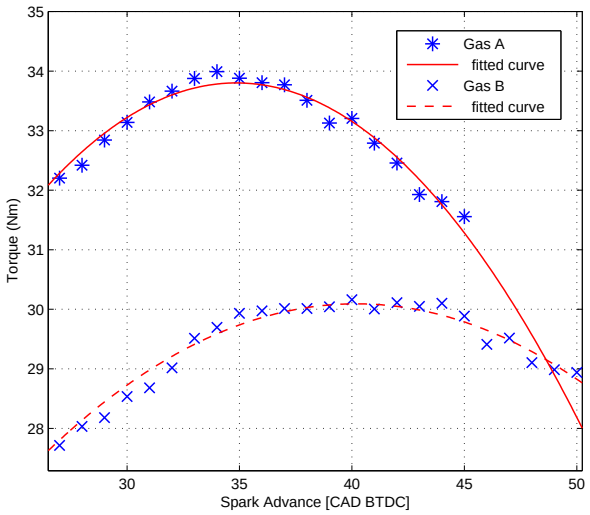

Fig. 6. Steady-state mapping between the spark advance and brake torque for Gas A (solid line) and Gas B (dashed line) at engine operating point of 800rpm and 30Nm - CAD BTDC means Crank Angle Degrees Before Top-Dead Center

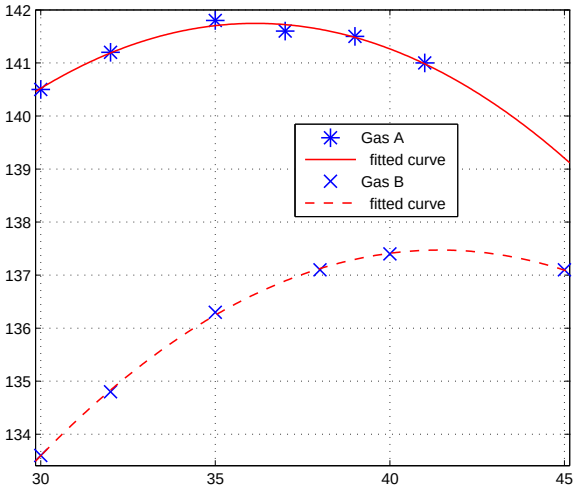

Fig. 7. Steady-state mapping between the spark advance and brake torque for Gas A (solid line) and Gas B (dashed line) at engine operating point of 1500rpm and 140Nm - CAD BTDC means Crank Angle Degrees Before Top-Dead Center

Open loop tests were performed at two different operating points, one at close to idle engine condition of 800rpm, 30Nm and the other one at higher load and speed of 1500rpm and 140Nm. All test are conducted at stoichiometric air/fuel ratio. In these tests, for each gas composition, the brake torque is measured for different spark advances. Fig. 6 and 7 show the open-loop test results for two natural gas compositions introduced in the previous section at two operating point of (800rpm,30Nm) and (1500rpm,140Nm), respectively. The spark advance sweeps with increment of 1 CAD shows MBT spark timing of 34 CAD BTDC for Gas A and 40 CAD BTDC for Gas B at operating point of (800rpm,30Nm) and 35 CAD BTDC for Gas A and 41 CAD BTDC for Gas B at operating point of (1500rpm,140Nm).

The results of the experiments were expected as the spark timing for Gas A need to advance because the inert gases (Nitrogen and Carbon Dioxide) slow down the development of the flame. Therefore, the spark timing of the engine for the gas with more inert gases should be advanced in order to provide sufficient time for the flame development. These results are similar to those observed in the study by Kim et al. (2009).

As depicted in Fig. 6 and 7, when the spark advance is calibrated at MBT for Gas B while the engine operates with Gas A, there is about 3% and 1% reduction in the brake torque of Gas A, respectively.

5.2 Plant description

In order to apply the grey-box ES controller to adjust the spark advance, a parameterized model of the mapping between the spark advance and the brake torque is required. The approach used here tries to find the polynomial of best fit for experimental data obtained from open-loop tests.

The Curve Fitting Toolbox of MATLAB was used to fit several polynomial models to the experimental data of Fig. 6 and 7 for Gas A and Gas B and in two operating points of the engine. The statistical evaluation of different polynomial fits demonstrates that there is no significant difference between different polynomial fits. However, the lower order polynomials are preferred as less parameters have to be estimated and therefore potentially can improve the speed of the grey-box ES controller. As a result, the parameterized model is chosen to be represented by a quadratic function; i.e.:

$$\begin{aligned}\tau &= a\alpha_{sa}^2 + b\alpha_{sa} + c \\ &= h(\theta, \alpha_{sa}) \end{aligned} \tag{23}$$

where τ is the engine brake torque, α_{sa} is the spark advance, $\theta = [a\ b\ c]^T$ is the unknown parameters vector and a, b, c are unknown, nominally constant parameters for a given fuel composition. By introducing $\phi = [\alpha_{sa}^2\ \alpha_{sa}\ 1]^T$, (23) can be written in the following compact form:

$$\tau = \phi^T(\alpha_{sa})\theta \tag{24}$$

Two curves in Fig. 6 correspond values for unknown parameters vector $\theta^T = [a\ b\ c]$ as $\theta_A^T = [-0.024\ \ 1.71\ \ 3.97]$ and $\theta_B^T = [-0.013\ \ 1.05\ \ 8.84]$. The corresponding values in Fig. 7 are $\theta_A^T = [-0.029\ \ 2.46\ \ 90.50]$ and $\theta_B^T = [-0.032\ \ 2.34\ \ 95.39]$. These set of parameters are obtained via fitting quadratic curves to the mappings of Fig. 6 and 7 for gas compositions Gas A and Gas B.

5.3 Discrete-time ES controller

Since the parameterized model of the plant is obtained in the previous subsection, using recursive least-squares algorithm (11a), (11b) for the estimator (EA4) and Jacobian matrix transpose method (15) for the optimizer (OA3), now assumptions of Theorem 1 can be verified. Assumption 1 holds since in the estimator (11a), (11b), the vector $\phi(\alpha_{sa})$ in (24) satisfies persistency of excitation (PE) condition (13) with the dither signal $d(t) = \sin(t)$

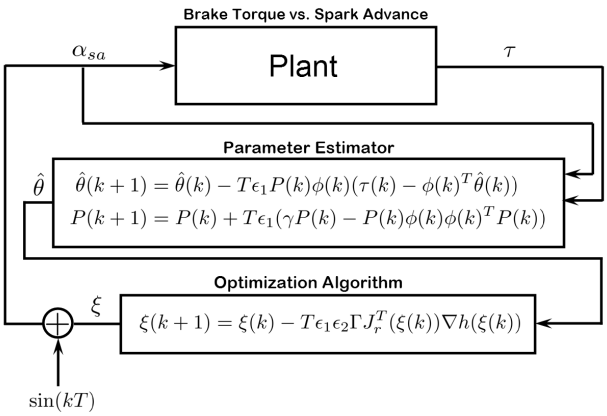

Fig. 8. Spark advance optimization block diagram for engines with varying fuel composition

and in the optimizer (15) Jacobian matrix $J_r(\xi) = 2a$ is obviously invertible as $a \neq 0$.

To verify Assumption 2, the Euler method is used to discretize the continuous-time controller (11a), (11b) and (15) which provides discrete-time model of the controller in coordinates $\tilde{\theta} = \hat{\theta} - \theta$, $\widetilde{P} = P - P^*$ and $\tilde{\xi} = \xi - \xi^*$ as:

$$\begin{aligned}
\tilde{\theta}(k+1) &= \tilde{\theta}(k) + T\epsilon_1 \widetilde{G}(\tilde{\theta}(k), \widetilde{P}(k), \tilde{\xi}(k)) \\
&= \widetilde{G}_T^a(\tilde{\theta}(k), \widetilde{P}(k), \tilde{\xi}(k), \epsilon_1), \qquad (25a) \\
\widetilde{P}(k+1) &= \widetilde{P}(k) + T\epsilon_1 \widetilde{H}(\widetilde{P}(k), \tilde{\xi}(k)) \\
&= \widetilde{H}_T^a(\widetilde{P}(k), \tilde{\xi}(k), \epsilon_1), \qquad (25b) \\
\tilde{\xi}(k+1) &= \tilde{\xi}(k) + T\epsilon_1\epsilon_2 \widetilde{F}(\tilde{\theta}(k), \tilde{\xi}(k)) \\
&= \widetilde{F}_T^a(\tilde{\theta}(k), \tilde{\xi}(k), \epsilon_1\epsilon_2). \qquad (26)
\end{aligned}$$

Then, regarding Definition 1:

- $\widetilde{G}_T^a$, $\widetilde{H}_T^a$ and $\widetilde{F}_T^a$ are obviously one-step consistent with $\widetilde{G}_T^{Euler}$, $\widetilde{H}_T^{Euler}$ and $\widetilde{F}_T^{Euler}$ as Euler method is used for discretization,
- $\widetilde{G}$, $\widetilde{H}$ and $\widetilde{F}$ are upper bounded and derivatives of $\widetilde{G}$ w.r.t $\tilde{\theta}$, $\widetilde{H}$ w.r.t $\widetilde{P}$ and $\widetilde{F}$ w.r.t $\tilde{\xi}$ are bounded.

Therefore, both assumptions of Theorem 1 hold and it can be concluded that by tuning the parameters ϵ_1, ϵ_2 and T, the approximate discrete-time closed-loop system (25a), (25b) and (26) has the property (22). Fig. 8 shows the spark advance optimization scheme using particular parameter estimator and optimization algorithm described above.

6. SIMULATION RESULTS

In this section, the designed discrete-time ES controller is applied to the plant model of Fig. 6 which corresponds to operating point of 800rpm and 30Nm. Implementation of controller for the other operating point in Fig. 7 delivers similar results which is not included here due to the space problem. The objective of controller is to find the MBT spark advance as fuel composition varies from Gas B to Gas A and vice versa. For this purpose, it is assumed that initially the engine is calibrated for Gas B, therefore, the spark advance is initialized from $\alpha^*_{sa(GasB)} = \xi(0) =$ 41 CAD BTDC (Crank Angle Degrees Before Top-Dead

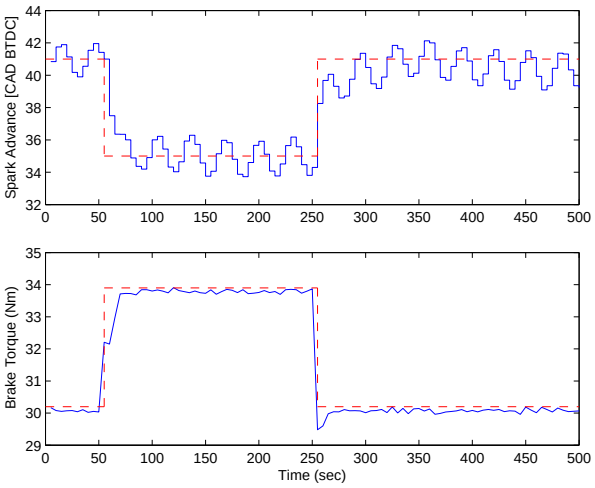

Fig. 9. Simulation results of the discrete-time grey-box ES controller in the presence of zero-mean white noise - Red dashed lines shows optimum values

Center). Then, after 50sec the fuel composition changes to Gas A. As a result, the controller should drive the spark advance to MBT spark advance of Gas A at $\alpha^*_{sa(GasA)} = 35$ CAD BTDC. Again after 250sec the fuel composition changes to Gas B and ES controller locates the MBT spark advance of Gas B at $\alpha^*_{sa(GasB)} = 41$. The unknown parameters are initialized at $\hat{\theta}(0) = [-0.013 \quad 1 \quad 8]^T$. In the estimation algorithm (11a) and (11b), the covariance matrix is initialized at $P(0) = 500I_{3\times3}$ and $\gamma = 0.9$. The dither signal used here is the sinusoidal signal $d(t) = \sin(t)$. The sample time is chosen as $T = 5sec$ similar to the required sample time in the experiments.

From practical standpoint, due to the cyclic variability, the indicated mean effective pressure (IMEP) is varying and consequently the brake torque. The coefficient of variation of IMEP is typically used to quantify the cycle-to-cycle variation, defined as the standard deviation of IMEP divided by the mean IMEP and it is usually in percent. Based on the experimental tests, for both Gas A and Gas B, the coefficient of variation of IMEP was about 0.7% in the region of optimum points. Therefore, based on obtained data in the experimental tests a zero-mean white noise with variance of 1 is added to the output torque of the plant to mimic the real engine measurements of the brake torque.

While zero-mean noise superimposed on the feedback measurements will not affect the steady state results, in practice it is typically desirable to reduce the gains in order to provide more uniform convergence to the extremum. This reduction has a direct impact on the convergence rate. In this work, the noise on torque measurements was handled by averaging the torque measurement over a period of three seconds.

Fig. 9 shows simulation results of the spark advance and the corresponding value of the brake torque. The discrete-time grey-box ES controller achieves the values of 35 CAD BTDC and 41 CAD BTDC for spark advance, respectively and holds these values with minor oscillations around the optimum points which are caused by the dither signal. The

amplitude and frequency of the dither signal are tuned in order to achieve the desired trade-off between convergence speed and accuracy. Note that other types of dither signals are possible (e.g. square wave, triangle, ...), see Tan et al. (2008), as long as the required conditions of Theorem 1 holds.

Up to this point, the results are only provided for the particular estimation and optimization algorithms while, as mentioned in Introduction, a large class of estimators can be combined with a large class of optimizers in the proposed grey-box ES framework. As a result, closed-loop performance of different combinations of parameter estimators and optimization algorithms are investigated. To this end, first a fair assessment criterion should be employed. The criterion used here is based upon a modified version of the average power loss (APL) proposed by Scotson and Wellstead (1990). In this criterion, the mean deviation of the actual engine brake torque, τ, from its achievable maximum, τ^* is accumulated over an operating span. Thus, the average power loss over $[k_0T, kT]$ is defined as

$$APL(k_0, k) = \frac{1}{(k - k_0)} \sum_{i=k_0}^{k} [\tau^* - \tau(i)] \qquad (27)$$

Typically, the APL is normalized by expressing it as a percentage of the maximum achievable performance, τ^*; therefore, the values in Table 3 are in terms of $\%APL$, i.e.:

$$\%APL(k_0, k) = \frac{APL(k_0, k)}{\tau^*} \times 100, \qquad (28)$$

where τ^* is the maximum torque.

Table 3. Performance comparison of different combination of estimators and optimizers regarding %APL for the first 50sec through simulations

	OA1	OA2	OA3	OA4	OA5	OA6
EA1	1.2	0.81	0.87	1.1	0.87	0.86
EA2	0.78	0.83	0.82	0.98	0.85	0.84
EA3	0.81	0.79	0.78	0.91	0.80	0.79
EA4	0.86	0.76	***0.73***	1	0.74	0.73
Without ES	2.7					

Table 3 shows the percentage of APL for different combinations of optimization algorithms (OA) and estimation algorithms (EA) considering the time span from $50sec$ to $100sec$ which corresponds to $k = 10$. All combinations are tuned for the best performance. Some combinations lead to better closed-loop behavior for this particular problem of spark timing optimization. The %APL of the particular estimator and optimizer used in the previous section (EA4 and OA3) is highlighted in Table 3. Comparing the performance of this combination with the case that there is no ES controller, the result is about four times better. This came at no additional hardware cost and therefore, it is worthwhile to use grey-box ES control and to try different combinations to find the ES algorithm that has better performance for the problem in hand.

Different combinations of the optimizers and estimators are suited for different type of problems. The newly developed framework perspective of ES does allow multiple combinations of estimation and optimization algorithms although it does not tell the designer how to select an appropriate combination.

7. EXPERIMENTAL RESULTS

The designed discrete-time grey-box ES controller was tested at the engine operating points of (800rpm,30Nm) and (1500rpm,140Nm). The sample time of the controller in all of the experimental tests is 5sec. For each iteration of the controller, the ES algorithm waits for two seconds after changing spark angle, then averages the brake torque signal for three seconds.

There are five parameters in the discrete-time ES controller to be tuned: sample time, adaptation gain in the parameter estimation algorithm, optimization rate in the optimizer, and frequency and amplitude of the dither signal. After choosing an appropriate sample time based on the system dynamics and the available hardware, the adaptation gain in the estimator and optimizer are chosen to make the system stable. Then, the amplitude of the dither signal starts with a big value and then decreases while dither frequency starts with small value and increases such that the convergence speed and accuracy are acceptable. These values highly depend on the sensitivity of the brake torque to change in the spark advance.

In the first set of the experiments, the engine operating point is maintained at 800rpm and 30Nm. The parameter estimation and optimization algorithms are considered the same as simulation (EA4 as estimator and OA3 as optimizer). The initial conditions are $\alpha_{sa}(0) = \xi(0) = 41$, $\theta(0) = [-0.013 \quad 1 \quad 8]$, and $P(0) = 500I$. The ES perturbation frequency and amplitude are $\omega = 0.2$ and $a = 1$.

Fig. 10 shows that the spark angle converges to its optimum value at $\alpha^*_{sa} = 35$ CAD BTDC in less than 20 seconds. The transient response of the proposed ES controller is mainly depends on the initial conditions of the parameter estimation algorithm and the combination of the estimator and optimizer used in the controller. Moreover, as depicted in Fig. 10, after convergence to optimum spark advance it is still oscillating around the optimum value due to the dither signal required for the parameter estimation. Any loss due to the dither oscillations after convergence is masked by cyclic variations in brake torque.

In order to show the flexibility of the framework, Jacobian matrix transpose method is replaced by gradient method with the same initial conditions. The result is shown in Fig. 11. Also, the combination of gradient method as estimator and Jacobian matrix transpose as optimizer has been shown in Fig. 12.

The tests are repeated for the engine operating condition of 1500rpm and 140Nm. The tuning parameters are similar to the previous operating point. Fig. 13-15 depict the experimental results for different combination of parameter estimation and optimization algorithms. The results show that in this new operating point the controller can drive the spark advance to its optimum point. Note that fixed gains are used throughout the tests for different operating points although there is possibility that conservative tun-

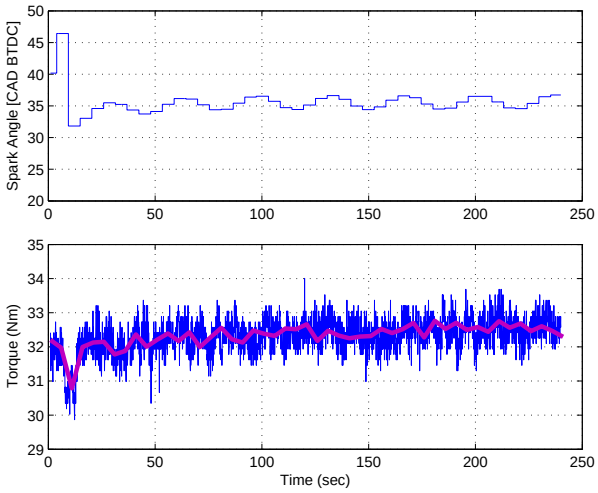

Fig. 10. Grey-box ES controller performance for the spark timing calibration using RLS (EA4) as estimator and Jacobian matrix transpose method (OA3) as optimizer at 800rpm and 30Nm - Thick pink line shows the averaged torque used by ES controller

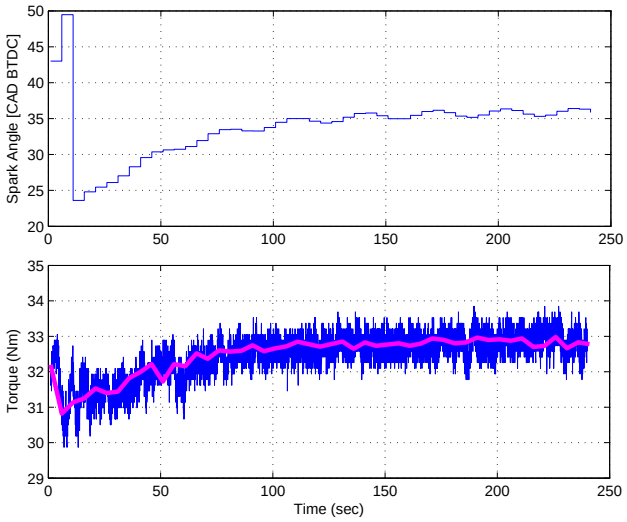

Fig. 11. Grey-box ES controller performance for the spark timing calibration RLS (EA4) as estimator and gradient method (OA1) as optimizer at 800rpm and 30Nm

ing of parameters are required to achieve stability over the entire engine operating point.

Table 4 shows the performance of different combinations of optimization and estimation algorithms and a few other combinations at two different operating points. The combination of the estimator EA4 and optimizer OA3 has better APL in comparison to the other combinations as expected from simulation results in Table 3.

To quantitatively measure the influence of ES on potential fuel economy, the engine was run using Gas A and the calibration for Gas B. This represents the benchmark where no adaptation takes place and the fuel flow rate was measured. When the ES is switched on, the spark is adapted and the torque increases as the MBT spark is

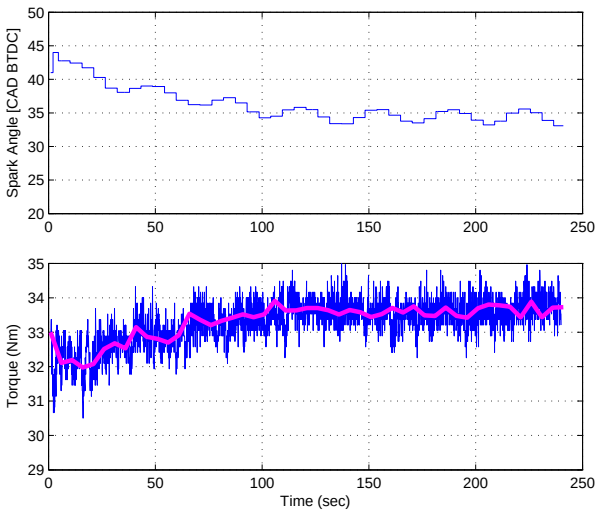

Fig. 12. Grey-box ES controller performance for the spark timing calibration using gradient method (EA1) as estimator and Jacobian matrix transpose method (OA3) as optimizer at at 800rpm and 30Nm

Table 4. Performance comparison of some combinations of estimators and optimizers regarding %APL for the first 200sec through experiments

	800rpm/30Nm			1500rpm/140Nm		
	OA1	OA2	OA3	OA1	OA2	OA3
EA1	1.57	1.41	1.35	0.95	0.82	0.87
EA4	1.24	1.12	0.92	0.75	0.63	0.55
Without ES	2.5			1.5		

gradually identified. Without the dynamometer in place to absorb the load, this would lead to an increase in speed - something a driver or ECU would correct through throttle adjustment. Under an assumption of stoichiometric air fuel ratio at both operating points, the reduction in throttle angle correlates with a decrease in fuel use of 1% and 3% at the two operating points considered.

The experiments considered in this work are restricted to single operating points of the engine in order to demonstrate the asymptotic convergence of the proposed approach. Of course, in real transient operation, separate spark timing setpoints can be independently updated using the proposed approach with appropriate synchronization of the inputs and output measurements.

8. CONCLUSIONS

This contribution demonstrated the feasibility of applying grey-box extremum seeking framework in practical engineering problems. In particular, the grey-box ES framework is utilized to design a controller for online optimization of spark advance in automotive engine. This is primarily of interest in alternative fueled engines due to the varying composition of the fuel. The simulation results showed that the grey-box ES controller is robust enough to cope with this situation. This paper also demonstrated the flexibility of the framework by using different parameter

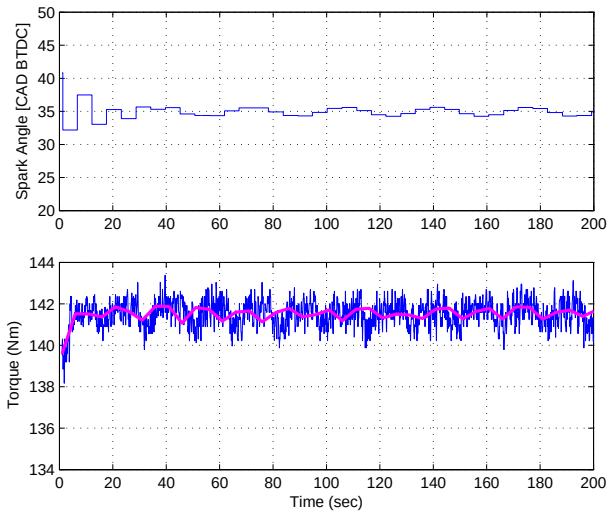

Fig. 13. Grey-box ES controller performance for the spark timing calibration using RLS (EA4) as estimator and Jacobian matrix transpose method (OA3) as optimizer at 1500rpm and 140Nm

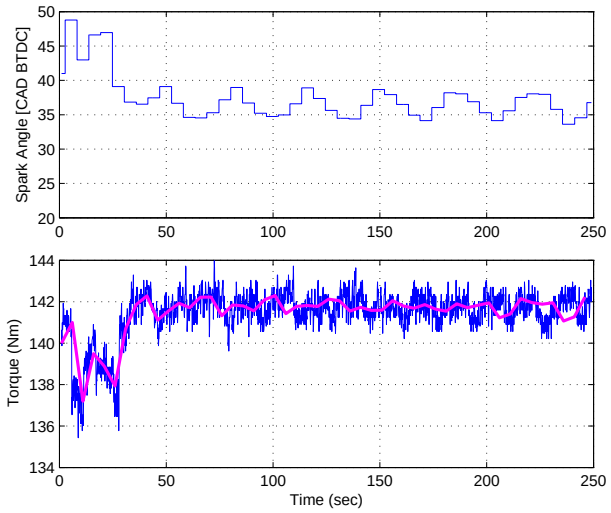

Fig. 14. Grey-box ES controller performance for the spark timing calibration RLS (EA4) as estimator and gradient method (OA1) as optimizer at 1500rpm and 140Nm

estimators and optimization algorithms. The grey-box ES controller presented in this paper is used in experiments on a CNG fueled engine to adjust the spark advance online as the fuel composition changes.

For the future work, due to cylinder-to-cylinder variations, a MIMO and MISO type of the proposed ES controller can be implemented where each cylinder is optimized separately and this may provide some additional improvements.

Appendix A. PROOF OF THEOREM 1

The proof of Theorem 1 follows the same steps as that of Theorem 3.1 in Laila et al. (2002). The only difference is

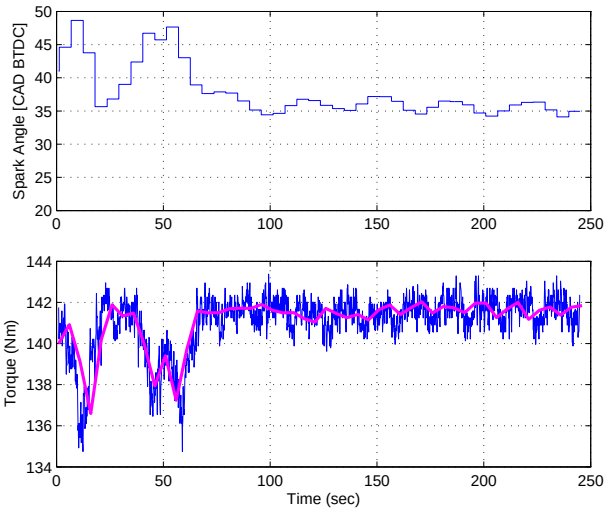

Fig. 15. Grey-box ES controller performance for the spark timing calibration using gradient method (EA1) as estimator and Jacobian matrix transpose method (OA3) as optimizer at 1500rpm and 140Nm

that here there are two tuning parameters, ϵ_1 and ϵ_2, that should be included in the conditions for obtaining T^*.

Let a 8-tuple of strictly real numbers $(\Delta_{\tilde{x}}, \Delta_{\tilde{\theta}}, \Delta_{\tilde{\eta}}, \Delta_{\tilde{\eta}}, \Delta_d, \Delta_{\dot{d}}, \hat{\nu}, \nu)$ be given. Let these data generate $\rho_1, \rho_2 \in \mathcal{K}_\infty$ from the definition of the one-step consistency. Define $\mathcal{R}_{\tilde{x}} := \Delta_{\tilde{x}} + 1$, $\mathcal{R}_{\tilde{\theta}} := \Delta_{\tilde{\theta}} + 1$, $\mathcal{R}_{\tilde{\eta}} := \Delta_{\tilde{\eta}} + 1$ and $\mathcal{R}_{\tilde{\xi}} := \Delta_{\tilde{\xi}} + 1$. Let $L > 0$ be the Lipschitz constant of $\widetilde{f}$, $\widetilde{G}$, $\widetilde{H}$ and $\widetilde{F}$ on the sets where $|\tilde{x}| \leq \mathcal{R}_{\tilde{x}}$, $|\tilde{\theta}| \leq \mathcal{R}_{\tilde{\theta}}$, $|\tilde{\eta}| \leq \mathcal{R}_{\tilde{\eta}}$, $|\tilde{\xi}| \leq \mathcal{R}_{\tilde{\xi}}$, $|d| \leq \Delta_d$. Let $b > 0$ be a number that satisfies $\max\left\{|\frac{\partial V}{\partial \tilde{x}}|, \left|\frac{\partial V}{\partial \tilde{\theta}}\right|, \left|\frac{\partial V}{\partial \tilde{\eta}}\right|, \left|\frac{\partial V}{\partial \tilde{\xi}}\right|, |\widetilde{f}|, |\widetilde{G}|, |\widetilde{H}|, |\widetilde{F}|\right\} \leq b$ for all $\tilde{x} \leq \mathcal{R}_{\tilde{x}}$, $\tilde{\theta} \leq \mathcal{R}_{\tilde{\theta}}$, $\tilde{\eta} \leq \mathcal{R}_{\tilde{\eta}}$, $\tilde{\xi} \leq \mathcal{R}_{\tilde{\xi}}$, $d \leq \Delta_d$. Define $\Delta := \Delta_{\tilde{x}} + \Delta_{\tilde{\theta}} + \Delta_{\tilde{\eta}} + \Delta_{\tilde{\xi}} + \Delta_d$.

It is assumed without loss of generality that $\hat{\nu} \leq 1$ and $b \geq 1$ and define

$$T_1^* := \min\left\{\frac{1}{4b}, \rho_1^{-1}\left(\frac{\hat{\nu}}{4b}\right), \rho_2^{-1}\left(\frac{\hat{\nu}}{4b}\right)\right\}$$

Note that $T_1^* \leq \frac{1}{4b} \leq \frac{1}{4} < 1$.

Let $T_2^* > 0$ be such that the following holds:

$$\epsilon_1^* bL\left[(\Delta+1)\frac{\exp(LT)-1-LT}{LT} + \frac{1}{2}\Delta_{\dot{d}}T\right] \leq \frac{\hat{\nu}}{32} \qquad \forall T \in (0, T_2^*) \tag{A.1}$$

Let $T_3^* > 0$ be such that the following holds:

$$\epsilon_1^*\epsilon_2^* bL\left[(\Delta+1)\frac{\exp(LT)-1-LT}{LT} + \frac{1}{2}\Delta_{\dot{d}}T\right] \leq \frac{\hat{\nu}}{32} \qquad \forall T \in (0, T_3^*) \tag{A.2}$$

Let $\tilde{x}_1 := \widetilde{f} + \gamma_1 T\widetilde{f}$, $\tilde{\theta}_1 := \tilde{\theta} + \gamma_2 T\widetilde{G}$, $\tilde{\eta}_1 := \tilde{\eta} + \gamma_3 T\widetilde{H}$, $\tilde{\xi}_1 := \tilde{\xi} + \gamma_4 T\widetilde{F}$ where $\gamma_1, \gamma_2, \gamma_3, \gamma_4 \in (0, 1)$.

Let $T_4^* > 0$, $T_5^* > 0$, $T_6^* > 0$ and $T_7^* > 0$ such that:

$$b\left|\frac{\partial V}{\partial \tilde{x}}|_{(\tilde{x}_1,\tilde{\theta}+T\epsilon_1\widetilde{G},\tilde{\eta}+T\epsilon_1\widetilde{H},\tilde{\xi}+T\epsilon_1\epsilon_2\widetilde{F})}-\frac{\partial V}{\partial \tilde{x}}|_{(\tilde{x},\tilde{\theta},\tilde{\eta},\tilde{\xi})}\right| \leq \frac{\hat{\nu}}{32}, \qquad \forall T\in(0,T_4^*) \tag{A.3}$$

$$\epsilon_1^* b\left|\frac{\partial V}{\partial x_m}|_{(\tilde{x},\tilde{\theta}_1,\tilde{\eta}+T\epsilon_1\widetilde{H},\tilde{\xi}+T\epsilon_1\epsilon_2\widetilde{F})}-\frac{\partial V}{\partial x_m}|_{(\tilde{x},\tilde{\theta},\tilde{\eta},\tilde{\xi})}\right| \leq \frac{\hat{\nu}}{32}, \qquad \forall T\in(0,T_5^*) \tag{A.4}$$

$$\epsilon_1^* b\left|\frac{\partial V}{\partial x_m}|_{(\tilde{x},\tilde{\theta},\tilde{\eta}_1,\tilde{\xi}+T\epsilon_1\epsilon_2\widetilde{F})}-\frac{\partial V}{\partial x_m}|_{(\tilde{x},\tilde{\theta},\tilde{\eta},\tilde{\xi})}\right| \leq \frac{\hat{\nu}}{32}, \qquad \forall T\in(0,T_6^*) \tag{A.5}$$

$$\epsilon_1^*\epsilon_2^* b\left|\frac{\partial V}{\partial x_s}|_{(\tilde{x},\tilde{\theta},\tilde{\eta},\tilde{\xi}_1)}-\frac{\partial V}{\partial x_s}|_{(\tilde{x},\tilde{\theta},\tilde{\eta},\tilde{\xi})}\right| \leq \frac{\hat{\nu}}{32}, \qquad \forall T\in(0,T_7^*) \tag{A.6}$$

for all T_4^*, T_5^*, T_6^* and T_7^*.

Finally, T^* is defined as

$$T^* := \min\{T_1^*, T_2^*, T_3^*, T_4^*, T_5^*, T_6^*, T_7^*\}.$$

Considering conditions (A.1)-(A.6), the rest of proof follows the same steps of Laila et al. (2002).

REFERENCES

Draper, C. S. and Li, Y. Principles of Optimizing Control Systems. ASME Publications, 1954.

Egardt, B. and Larsson, S., On a Parameter Adaptive Extremum Controller. *IEEE Control and Decision Conference*, Seville, Spain, December 12-15, 2005.

Eriksson, L. Spark advance for optimal efficiency. *SAE Paper*, 1999-01-0548, 1999.

Glaser, I. and Powell, J. D. Optimal closed-loop spark control of an automotive engine. *SAE Paper*, 810058, 1981.

Hellström, E., Lee, D., Jiang, L., Stefanopoulou, A. G. and Yilmaz, H. On-Board Calibration of Spark Timing by Extremum Seeking for Flex-Fuel Engines. *IEEE Transaction on Control Systems Technology*, DOI:10.1109/TCST.2012.2236093.

Killingsworth, N.J., Aceves, S.M., Flowers, D.L., Espinosa-Loza, F. and Krstic, M. HCCI Engine Combustion-Timing Control: Optimizing Gains and Fuel Consumption Via Extremum Seeking. *IEEE Transactions on Control Sys. Tech.*, vol. 17, No. 6, pp. 1350-61, 2009.

Kim, K., Kim, H., Kim, B., Lee, K. and Lee, K. Effect of Natural Gas Composition on the Performance of a CNG Engine. *Oil and Gas Science and Technology Rev. IFP*, Vol. 64, No. 2, pp. 199-206, 2009.

Ariyur, K. B. and Krstić, M. *Real-Time Optimization by Extremum-Seeking Control*, Wiley-Interscience, A John Wiley & Sons, Inc., Publication, 2003.

Laila, D. S., Nešić, D. and Teel, A. Open and closed loop dissipation inequalities under sampling and controller emulation. *European Journal of Control*, Vol. 8, No. 12, pp. 119-125, 2002.

Larsson, S. and Andersson, I. Self-optimising control of an SI-engine using a torque sensor. *Control Engineering Practice*, Vol. 16, No. 5, pp. 505-514, 2008.

Leonhardt, S., Muller, N. and Isermann, R. Methods for engine supervision and control based on cylinder pressure information. *IEEE/ASME Transactions on Mechatronics*, Vol. 4, No. 3, pp. 235-245, 1999.

Lewander, M., Widd, A., Johansson, B. and Tunestal, P. Steady state fuel consumption optimization through feedback control of estimated cylinder individual efficiency. *IEEE American Control Conference*, pp. 4210-14, 2012.

Ly, H. Effects of Natural Gas Composition Variations on the Operation Performance and Exhaust Emissions of Natural Gas-Powered Vehicles. *Proc. NGV Conf.*, 2002.

Min, B., Bang, K. and Kim, H. Effects of Gas Composition on the Performance and Hydrocarbon Emissions for CNG Engines. *SAE paper*, No. 981918, 1998.

Mohammadi, A., Nešić, D. and Manzie, C., Extremum Seeking Methods for Online Optimization of Spark Advance in Alternative Fueled Engines. *Proceedings of Engine and Powertrain Control, Simulation and Modeling*, Vol. 3, No. 1, pp. 1-8, 2012.

Nešić, D. Extremum seeking control: convergence analysis. *Europ. J. Contr.*, vol. 15, No. 3-4, pp. 331-347, 2009.

Nešić, D., Mohammadi, A. and Manzie, C. A Framework for Extremum Seeking Control of Systems with Parameter Uncertainties. *IEEE Transactions on Automatic Control*, Vol.58, Issue 2, pp. 435-448, 2013.

Oostendorp, D. L. and Levinsky, H. B. The effects of fuel and non-fuel gases on the laminar burning velocity of methane-air flames. *Journal of the Institute of Energy*, Vol. 63, pp. 160-166, 1990.

Owens, D. H., Zheng, Y. and Billings, S. A. Fast sampling and stability of non-linear sampled-data systems: Part 1. Existence theorems. *IMA J. Math. Contr. Informat.*, Vol. 7, pp. 1-11, 1990.

Park, S. and Sunwoo, M. Torque estimation of spark ignition engines via cylinder pressure measurement. *Proceedings of the Institution of Mechanical Engineers, Part D: Journal of Automobile Engineering*, Vol. 217, No. 9, pp. 809-817, 2003.

Pierre, D. A. and Pierre, J. W. Digital controller design - Alternative emulation approaches. *ISA Transactions*, Vol. 34, pp. 219-28, 1995.

Popović, D., Janković, M., Magner, S. and Teel, A. R. Extremum Seeking Methods for Optimization of Variable Cam Timimg Engine Operation. *IEEE Trans. on Contr. Sys. Tech.*, Vol. 14, No. 3, pp. 398-407, 2006.

Qu, Z. *Robust control of nonlinear uncertain systems*, John Wiley & Sons: New York, 1998.

Scotson, P. and Wellstead, P. E. Self-tuning optimization of spark ignition automotive engines. *IEEE Control Sys. Mag.*, Vol. 3, No. 10, pp. 94-101, Apr. 1990.

Sivak, M. and Tsimhoni, O. Fuel efficiency of vehicles on US roads: 19232006. *Energy Policy*, Vol. 37, No. 8, pp. 3168-3170, 2009.

Soderstrom, T., Fan, H., Carlsson, B. and Bigi, S. Least squares parameter estimation of continuous-time ARX models from discrete-time data. *IEEE Transactions on Automatic Control*, Vol. 42, No. 5, pp. 659-673, 1997.

Tan, Y., Nešić, D., Mareels, I. M. Y. On the choice of dither in extremum seeking systems: A case study. *Automatica*, Vol. 44, No. 5, pp. 1446-50, 2008.

Tan, Y., Moase, W. H., Manzie, C., Nesic, D. and Mareels, I. M. Y. Extremum seeking from 1922 to 2010. *IEEE 29th Chinese Control Conference*, vol. 63, pp. 14-26, 2010.

Teel, A. R., Nešić, D. and Kokotović, P. V. A note on input-to-state stability of sampled-data nonlinear systems. Proceedings of *37th IEEE Conference on Decision and Control*, Vol. 3, pp. 2473-2478, 1998.

Zarrop, M. B. and Romments M. J. J. J. Convergence of a multi-input adaptive extremum controller. *IEE Proceedings Part D Control Theory and Applications*, Vol. 140, No. 2, pp. 65-69, Apr. 1993.